RESEARCH ARTICLE

Key Points:
- Dissipating planetary waves (PWs) in the MLT can drive background wind changes
- Mixing from dissipating PWs drive thermosphere/ionosphere composition changes
- First observations of QTDW-driven variability from this mechanism

Correspondence to:
L. C. Chang,
loren@jupiter.ss.ncu.edu.tw

Quasi two day wave-related variability in the background dynamics and composition of the mesosphere/ thermosphere and the ionosphere

Loren C. Chang[1], Jia Yue[2], Wenbin Wang[3], Qian Wu[3], and R. R. Meier[4]

[1]Institute of Space Science, National Central University, Jhongli, Taiwan, [2]Center for Atmospheric Science, Hampton University, Hampton, Virginia, USA, [3]High Altitude Observatory, National Center for Atmospheric Research, Boulder, Colorado, USA, [4]School of Physics, Astronomy, and Computational Sciences, George Mason University, Fairfax, Virginia, USA

Abstract Dissipating planetary waves in the mesosphere/lower thermosphere (MLT) region may cause changes in the background dynamics of that region, subsequently driving variability throughout the broader thermosphere/ionosphere system via mixing due to the induced circulation changes. We report the results of case studies examining the possibility of such coupling during the northern winter in the context of the quasi two day wave (QTDW)—a planetary wave that recurrently grows to large amplitudes from the summer MLT during the postsolstice period. Six distinct QTDW events between 2003 and 2011 are identified in the MLT using Sounding of the Atmosphere using Broadband Emission Radiometry temperature observations. Concurrent changes to the background zonal winds, zonal mean column O/N_2 density ratio, and ionospheric total electron content (TEC) are examined using data sets from Thermosphere Ionosphere Mesosphere Energetics and Dynamics Doppler Interferometer, Global Ultraviolet Imager, and Global Ionospheric Maps, respectively. We find that in the 5–10 days following a QTDW event, the background zonal winds in the MLT show patterns of eastward and westward anomalies in the low and middle latitudes consistent with past modeling studies on QTDW-induced mean wind forcing, both below and at turbopause altitudes. This is accompanied by potentially related decreases in zonal mean thermospheric column O/N_2, as well as to low-latitude TECs. The recurrent nature of the above changes during the six QTDW events examined point to an avenue for vertical coupling via background dynamics and chemistry of the thermosphere/ionosphere not previously observed.

1. Introduction

Considerable advances have been made in understanding the mechanisms by which oscillations in the lower and middle atmosphere may produce variability in the thermosphere and ionosphere. The periodicities and zonal wave numbers of global-scale neutral atmospheric oscillations such as atmospheric tides, various propagating planetary waves (PWs) including ultrafast Kelvin waves, the quasi two day wave, as well as the 5, 10, and 16 day Rossby normal modes, have been observed in the thermosphere and the ionosphere. The persistent migrating atmospheric tides dominating the dynamics of the mesosphere/lower thermosphere (MLT) region can also be modulated by such propagating PWs through nonlinear interactions [*Teitelbaum and Vial*, 1991; *Pancheva*, 2000; *Liu et al.*, 2010]. These signatures of vertical coupling involve direct propagation of such neutral atmospheric oscillations into the thermosphere [*Forbes et al.*, 2009] or modulation of neutral winds and polarization electric fields in the ionospheric *E* region dynamo, thereby altering the equatorial fountain responsible for the equatorial ionization anomalies (EIAs) [*England et al.*, 2006] (hereafter referred to as the *E region dynamo mechanism*). With both of these mechanisms, the period and zonal wave number of the tide/PW, as well as higher-order harmonics due to modulation by diurnal variation, magnetic declination, or nonlinear interaction with atmospheric tides, manifests in ionospheric/thermosphere parameters [*Pancheva*, 2000; *Liu et al.*, 2010; *Chang et al.*, 2011b; *Pedatella et al.*, 2012b; *Yue et al.*, 2013a; *Onohara et al.*, 2013; *Chang et al.*, 2013b].

Another mechanism for vertical coupling between waves in the mesosphere/lower thermosphere (MLT) and the thermosphere/ionosphere involves momentum deposition from waves and tides dissipating in that region. The resulting changes to the background MLT dynamics from such wave drag subsequently induce global-scale changes to the dynamics and composition of the thermosphere/ionosphere (hereafter referred to as the *mixing mechanism*), particularly by producing increased mixing that depletes the thermosphere

of atomic oxygen, while increasing concentrations of molecular nitrogen and molecular oxygen, and is thus reflected as a decrease in the thermosphere O/N_2 volume (number) density mixing ratio [*Yue and Wang*, 2014], as well as the O/N_2 column density ratio. (We define the column number density ratio as $\Sigma O/N_2$ to distinguish from volume number density ratio.) This causes an increase in mean molecular mass, resulting in decreased mean thermospheric-scale height and decreased thermosphere neutral density at fixed altitudes [*Fuller-Rowell*, 1998; *Qian et al.*, 2009]. Atomic oxygen ions also have a longer lifetime in the ionospheric *F* region due to their slow radiative recombination rate, and reductions in the O/N_2 ratio result in faster plasma loss rates and reductions to ionospheric total electron content [*Fuller-Rowell*, 1998; *Yamazaki and Richmond*, 2013]. Unlike the direct propagation and *E* region dynamo mechanisms mentioned previously, changes resulting from this mixing mechanism do not show the period and wave number of wave/tide involved but are roughly proportional to the square of the amplitude of the wave/tide involved, likely due to a similar relation between wave/tidal amplitudes and their Eliasson-Palm flux divergence of zonal momentum [*Yamazaki and Richmond*, 2013].

The effects of increased mixing from the global-scale interhemispheric circulation during solstice were first proposed by *Fuller-Rowell* [1998] to explain the semiannual thermospheric density variation. This study established that the general circulation in the thermosphere could thus act to produce mixing in much the same way as a large-scale turbulent eddy (the "thermospheric spoon"). An earlier numerical study by *Forbes et al.* [1993] also explored the effects of tidal dissipation on the thermosphere, noting that the dissipation of the migrating diurnal tide in the lower thermosphere had the effect of forcing a westward zonal mean jet in the equatorial region, while depleting the thermosphere of atomic oxygen, increasing the concentration of molecular species and depleting electron densities above 160 km due to enhanced loss rates.

More recently, *Qian et al.* [2009] proposed that eddy mixing induced by breaking gravity waves on the MLT zonal mean zonal winds could subsequently produce changes to thermosphere neutral composition and showed through numerical experiments that the seasonal variation of such gravity wave drag could produce large contributions to the semiannual and annual variation in thermosphere neutral density. On a larger scale, the dominant migrating atmospheric tides are also known to be capable of producing westward wave drag on MLT zonal mean zonal winds [*Forbes et al.*, 1993] and can result in reductions to ionospheric zonal mean total electron content (TEC) directly proportional to the seasonal variation in tidal amplitudes in models [*Chang et al.*, 2013a]. *Yamazaki and Richmond* [2013] examined this mechanism in detail using numerical experiments, finding that westward forcing from the migrating tides could induce poleward meridional flow in both hemispheres of the lower thermosphere, as well as downwelling from the low-latitude thermosphere, and upwelling at higher latitudes. This induced circulation ultimately caused a reduction in the O/N_2 ratio due to the increased mixing (referred to in that study as tidal mixing), thereby increasing plasma loss rates.

Unlike the tides and gravity wave drag, which are generally persistent features changing mainly on seasonal scales, planetary wave activity can vary significantly on much shorter time scales of a few days, allowing for easier isolation of potentially related background changes. One such propagating PW is the quasi two day wave (QTDW), which has a period near 2 days and westward zonal wave number 3 (W3) during southern summer, mixed W3 and W4 during the northern summer, and smaller contributions from a W2 component [*Tunbridge et al.*, 2011]. The QTDW is known to amplify from the summer midlatitude upper stratosphere/lower mesosphere in the postsolstice period, extending upward and across the equator into the winter lower thermosphere [*Palo et al.*, 2007], with contributions from both the 3,0 (4,0) Rossby-gravity normal mode for the W3 (W4) component as well as baroclinic-barotropic instabilities [*Plumb*, 1983; *Pfister*, 1985; *Salby and Callaghan*, 2001; *Liu et al.*, 2004; *Tunbridge et al.*, 2011; *Yue et al.*, 2012a]. In contrast to northern summer QTDW events that show multiple bursts of activity within a single season, QTDW events occurring during the southern summer tend to manifest as a single impulsive burst of stronger amplitude, allowing its signatures to be isolated more easily [*Tunbridge et al.*, 2011].

The QTDW is known to be capable of coupling into the ionosphere via the *E* region dynamo mechanism. *Chen* [1992] and *Pancheva et al.* [2006] resolved the periodicity of the QTDW in ground-based observations of *F* region electron densities and ionospheric electric currents at the same time as QTDW events observed by MLT radar. Global-scale satellite observations have allowed the occurrence of such direct coupling to be elucidated with a further level of confidence. *Chang et al.* [2011b] isolated the global response of TECs to W3 and W2 QTDWs from GPS-derived Global Ionospheric Maps (GIM), which revealed a coherent

ionospheric response not only with the same frequency and zonal wave number as the QTDW in the MLT but also with similar hemispheric symmetry. *Pedatella and Forbes* [2012a] also resolved frequency and wave number signatures of the QTDW using global satellite observations of CHAMP in situ electron densities at 360 km at EIA latitudes, which were simultaneous with a W3 QTDW event found in Sounding of the Atmosphere using Broadband Emission Radiometry (SABER) MLT temperatures and OH airglow. Numerical experiments have shown similar results [*Yue et al.*, 2012b], as well as the splitting of the QTDW zonal wave number in the ionosphere due to magnetic declination effects [*Yue et al.*, 2013a].

In addition to the aforementioned *E* region dynamo mechanism, there is considerable evidence that the QTDW can drive major changes in MLT zonal mean zonal winds through westward momentum deposition and subsequent filtered gravity wave effects [*Palo et al.*, 1999; *Lieberman*, 1999; *Fritts et al.*, 1999; *Chang et al.*, 2011a]. These changes to the MLT background fields have consequences for MLT tidal variability, as well as the potential to induce dynamical and composition changes in the thermosphere/ionosphere via the mixing mechanism.

Recent numerical simulations by *Yue and Wang* [2014] showed that increased mixing arising from QTDW-induced mean wind changes in the MLT region can drive decreases in lower thermospheric O/N_2, which then propagate upward into the upper thermosphere, including the altitudes of the ionospheric F_2 peak, through molecular diffusion. Decreases in low-/middle-latitude electron density are subsequently seen due to increased plasma loss rates arising from the increase in molecular species. Although decreases in background ionospheric electron density potentially related to the QTDW can be seen in some past observations [*Chen*, 1992; *Chang et al.*, 2011b], such changes were not explicitly discussed and have not been explored in coordinated observational studies.

In this study, we present the results from six case studies of changes to the background meso-sphere/thermosphere and the ionosphere EIAs at the same time as the occurrence of W3 QTDW events in the MLT during the southern summer. Interannually consistent features of background variability are highlighted to elucidate the extent to which mixing from QTDW-induced general circulation changes play a role in thermosphere/ionosphere variability. Our results provide some of the first observational confirmation of the QTDW-induced thermospheric and ionospheric changes due to mixing that were identified by *Yue and Wang* [2014].

2. Methodology

In this study, we utilize global observations spanning the MLT, thermosphere, and ionosphere from four data sources: W3 QTDW events are identified in the MLT from SABER temperatures, changes to MLT background winds are examined using Thermosphere Ionosphere Mesosphere Energetics and Dynamics (TIMED) Doppler Interferometer (TIDI), changes to thermosphere mean column O/N_2 density ratio are observed using Global Ultraviolet Imager (GUVI), and changes to the strength of the EIAs are examined using GIM TECs.

2.1. SABER

The Sounding of the Atmosphere using Broadband Emission Radiometry (SABER) instrument aboard the TIMED (Thermosphere Ionosphere Mesosphere Energetics and Dynamics) satellite is a multichannel limb scan radiometer providing vertical profiles of atmospheric temperature and composition from 10 to 120 km, with continuous coverage equatorward of 50° geographic latitude [*Remsberg et al.*, 2003]. The QTDW structure is known to be manifested simultaneously in both wind and temperature fields in numerical experiments [*Palo et al.*, 1999; *Chang et al.*, 2011a], as well as in observations such as that using the Microwave Limb Sounder (MLS) aboard the Earth Observing System by *Limpasuvan and Wu* [2009], and in SABER and TIDI by *Gu et al.* [2013]. QTDW temperature amplitudes have also been used extensively in past studies due to the availability of temperature soundings over a broad vertical domain from instruments such as SABER [*Palo et al.*, 2007; *Chang et al.*, 2011b; *Moudden and Forbes*, 2014] and MLS [*Limpasuvan and Wu*, 2009; *Tunbridge et al.*, 2011], thus providing a large body of past work for intercomparison. Our results for the QTDW using SABER are consistent with these past studies.

In this study, we utilize SABER version 1.07 (http://saber.gats-inc.com) temperature observations to identify the spatial structure and time of occurrence for the W3 QTDW in the MLT region. We select an altitude of 85 km, which is close to the altitude of the lower QTDW amplitude peak at the mesopause and is more easily

resolved than the secondary peak in the lower thermosphere near 110 km [*Moudden and Forbes*, 2014]. Raw SABER temperature soundings at 85 km are binned into an overlapping geographic latitude × altitude grid of 2.5° × 2.5 km. The amplitudes and phases of the QTDW within a single bin are fitted using a linear least squares algorithm [*Wu et al.*, 1995] using a sinusoidal basis function with a period of 48 h and zonal wave numbers from E4 to W4.

SABER provides full longitude coverage within a single day, allowing for wave components of different zonal wave numbers to be effectively separated from each other [*Zhang et al.*, 2006]. In the time domain, we use a sliding window of 6 days, which is consistent with that used in past SABER QTDW studies [*Palo et al.*, 2007; *Chang et al.*, 2011b]. From sampling theory, we expect that our 6 day sliding window will provide a spectral resolution of 0.167 cpd (cycles per day). For the 48 h central period used to fit the QTDW in our study, we expect our fit to include a spectral range of 0.5 ± 0.167 cpd, corresponding to periods between 1.5 and 2.57 days. This is well within the known range of periods (1.85–2.17 days) for the QTDW identified in past studies, including the dominant W3 component and other identified components such as the W2 and E2 components [*Palo et al.*, 2007; *Limpasuvan and Wu*, 2009]. As such, our selected 6 day window combined with the use of multiple zonal wave numbers allows for QTDW components to be simultaneously extracted across this band pass, while still allowing for variability on the time scale of a few days to be identified.

2.2. TIDI

The TIMED Doppler Interferometer (TIDI) provides global measurements of horizontal neutral winds by measuring the Doppler shift of various airglow emissions using a limb scan Faby-Perot interferometer. The TIDI observations extend from pole to pole, capable of continuous day-night coverage between 80 and 105 km [*Killeen et al.*, 2006; *Wu et al.*, 2006]. Spectral analysis of TIDI horizontal wind measurement variances by *Yue et al.* [2013b] found uncertainties on the order of 2 m s^{-1} or less. Consistent with the SABER analysis, we select an altitude of 85 km, corresponding to the mesopause region peak of the W3 QTDW. The lower thermospheric W3 QTDW peak near 110 km exceeds the upper boundary of the TIDI observations.

TIDI zonal wind observations (http://timed.hao.ucar.edu/tidi/) are utilized in this study to determine changes in background zonal winds at 85 km and 100 km in the MLT region that occur with time scales on the order of those of a single QTDW event; these are potentially related to the presence of the QTDW. We utilize the background zonal winds for this study, as zonal mean meridional winds are considerably weaker than the zonal mean zonal winds, making the background meridional winds more susceptible to aliasing or other types of contamination. Retrieval of the background zonal winds is limited by the local time precession rate of the TIMED satellite orbit, which requires 63 days to cover 24 h of solar local time. The full local time coverage is required to unambiguously separate the tides, stationary PWs, and zonal mean components, so the TIMED orbital precession period is not useful for resolving changes shorter than those occurring on seasonal time scales.

We therefore utilize an alternative method of quantifying short time scale changes in background winds that exploits the fact that nonmigrating tides appear as stationary PWs when undersampled in local time [*Forbes et al.*, 2008]. We also take advantage of the separate local times of the ascending and descending passes of the TIMED satellite orbit. This is discussed in further detail in Appendix A.

The TIDI wind measurements are grouped within geographic latitude × height bins of 5° × 2.5 km. Because the TIDI samples on both the cold side (side of the spacecraft facing away from the Sun) and the warm side observation tracks are separated by roughly 180° longitude (or 12 h of local time) at latitudes other than the turning points near 45–60°, a zonal average within a single latitude/height bin incorporating both the ascending and descending legs will act to suppress DW1 (the migrating diurnal tide), as well as higher-order odd zonal wave number tides and stationary PWs. Since full longitude sampling is attained within a single day, averaging over a single day allows for the suppression of all stationary PWs and nonmigrating tides, the latter of which appear as stationary PWs when undersampled in local time [*Xu et al.*, 2013]. Thus, by performing zonal/time averaging at each latitude, we can suppress odd zonal wave number migrating tides, nonmigrating tides, and stationary PWs at low latitudes, even without full local time sampling.

The resulting background zonal winds in the low-latitude region include contributions from the zonal mean, even zonal wave number migrating tides (including SW2), and residuals of odd zonal wave number migrating tides (particularly DW1). Although SW2 (the migrating semidiurnal tide) cannot be removed without full local time sampling, the local time of the observations are constant interannually. A similar argument

applies for DW1 in the midlatitudes near the turning points where the local time separation of the ascending and descending legs of the individual tracks has larger deviations from 12 h, or during times when significant numbers of TIDI sample points are missing in the low latitudes. Despite this, the resulting background winds will still include contributions from zonal mean zonal winds altered by forcing from the QTDW.

To resolve potentially QTDW-induced MLT background wind changes on time scales of a few days, the aforementioned values are zonally averaged with a 6 day sliding window. As mentioned previously, the low-latitude background zonal winds contained in this 6 day zonal mean include the superposition of the zonal mean zonal winds, SW2, and some residuals from incomplete cancelation of DW1. Based on past TIDI studies of SW2 by *Wu et al.* [2011], contributions from SW2 will be located mainly at midlatitudes poleward of 50° latitude, attaining amplitudes as high as 48 m s^{-1} in the Northern Hemisphere during the southern summer. This allows us to mostly exclude contamination from SW2 in the low-latitude region. Residuals of DW1 will also be present, particularly at midlatitudes or during times of reduced sampling at low latitudes as mentioned previously. The former contamination should be mostly negligible as the peaks of DW1 in the MLT zonal wind fields are located around $\pm$ 20° latitude [*Wu et al.*, 2006]. While the latter cannot be entirely suppressed, the interannual consistency in the background zonal wind results shown later indicate that they do not dominate over QTDW-related changes. Additional discussion on the expected level of contamination from DW1 is in Appendix A.

2.3. GUVI

The Global Ultraviolet Imager (GUVI) is an imaging spectrometer that observes the FUV airglow in the 120–180 nm spectral range, on both the Earth limb and disk. *Christensen et al.* [2003] describe the GUVI instrument and operations. A mirror scans in a plane normal to the orbital track, commencing on the limb near 500 km tangent altitude on the side of the spacecraft away from the Sun. Every 15 s, the field of view is scanned downward across the disk, but not up to the limb on the sunward side in order to avoid viewing the Sun. Routine GUVI operation primarily consisted of limb and disk scanning from Day 60 of 2002 until Day 215 of 2007, when the scan mirror began to behave erratically. The scan mechanism failed entirely in December 2007, after 15 million scans.

Using the atomic oxygen 135.6 nm and N_2 Lyman-Birge-Hopfield (LBH) emission bands in the far ultraviolet, altitude profiles of N_2, O, and O_2 and temperature have been retrieved from the limb scan data; version 10 of the limb database is online at http://guvi.jhuapl.edu/site/data/guvi-dataproducts.shtml. Column O/N_2 density ratios (ΣO/N_2) are derived from the disk data, also online at the same site. The column density ratio is defined as the ratio of the vertical O column density to the N_2 column density, above the altitude where the N_2 column density is 10^{17} cm^{-2} (around 130–140 km, depending on solar activity). This provides the optimal algorithmic conversion from the disk 135.6 nm/LBH intensity ratio into ΣO/N_2 for comparison with models (details are given by *Strickland et al.* [1995]). Column density ratios are obtained from the limb data by numerically integrating the volume densities above this altitude. For the present work, we chose to use the limb ΣO/N_2 because the online disk values [*Zhang and Paxton*, 2011] are systematically lower than the limb values [*Meier et al.*, 2005] (also online at the above site) as well as being lower than the disk values obtained independently by *Strickland et al.* [2004]. In this study, raw ΣO/N_2 data are zonally averaged and binned into a geographic latitude grid of 5° width. Changes to thermospheric O/N_2 induced by the mechanism described by *Yue and Wang* [2014] will be reflected directly in the ΣO/N_2 observations [*Picone et al.*, 2013].

2.4. GIM

Global Ionosphere Maps (GIMs) of total electron content (TEC) are produced from assimilation of data from the global GPS/Global Navigation Satellite System receiver network by the Center for Orbit Determination in Europe (CODE) and are available via the International Global Navigation Satellite Systems Service [*Dow et al.*, 2009] (ftp://ftp.unibe.ch/aiub/CODE/). The resulting GIMs contain global snapshots of TEC with a geographic latitude $\times$ longitude resolution of 2.5$\times$5° every 2 h. In this study, the GIM TECs at each geomagnetic latitude are zonally averaged at all longitudes at 1600 h local time, which is representative of daytime conditions when the EIAs are strongest.

3. Results

In this study, we examine six W3 QTDW events identified from SABER temperatures during southern summers ranging from 2003 to 2011. We consider 90 days of each season from December to the end of February of the subsequent year. Only years with uninterrupted SABER coverage are considered. The amplitudes of
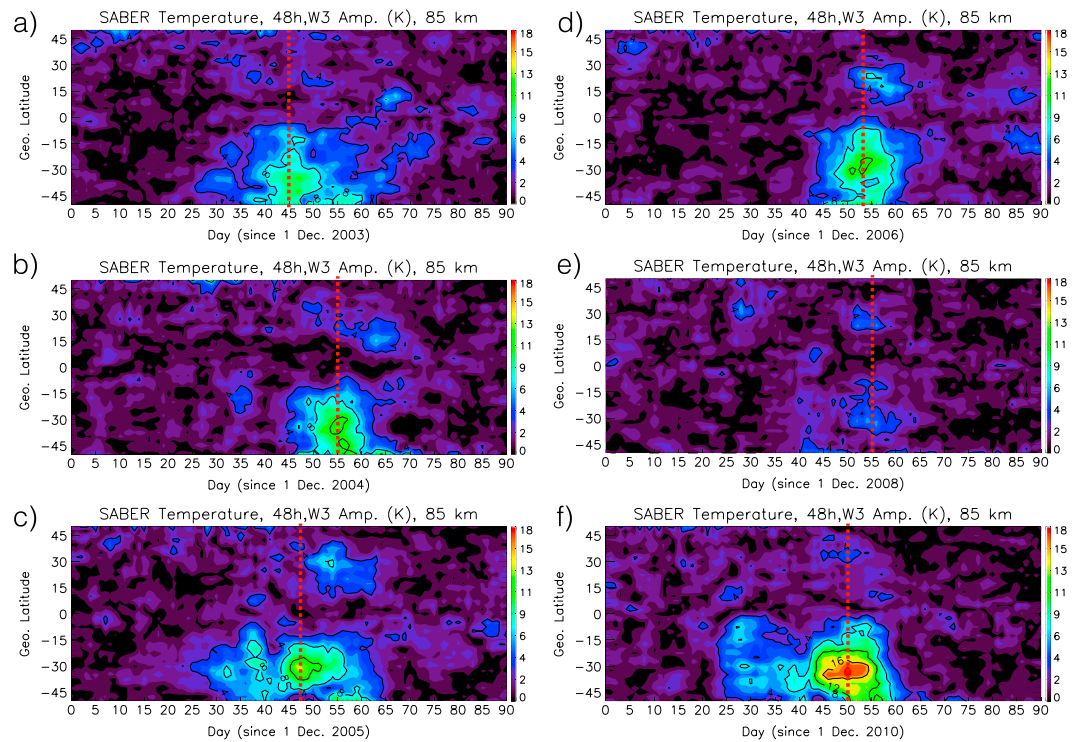
Figure 1. W3 QTDW amplitudes in SABER temperatures at 85 km as a function of geographic latitude and time for southern summers during (a) 2003/2004, (b) 2004/2005, (c) 2005/2006, (d) 2006/2007, (e) 2008/2009, and (f) 2010/2011. Day 0 corresponds to 1 December, day of peak QTDW amplitudes marked by dashed red line. Contour interval of 4 K.

the W3 QTDW in SABER temperatures at 85 km as a function of latitude and time are shown in Figure 1, with the peak days marked by a dashed red line and tabulated in Table 1.

The W3 QTDW events shown in Figure 1 exhibit features consistent with past studies, with maximum amplitudes occurring in the southern midlatitudes around 30–40°S during mid-January. The amplitudes extend across the equator into the northern midlatitudes around the same time during most of the years examined, in agreement with the structure of the 3,0 Rossby-gravity normal mode believed to account for the broad response of the W3 QTDW [*Yue et al.*, 2012a]. Considerable interannual variation in the magnitude of QTDW amplitudes is evident, with peak amplitudes as large as 17 K in 2010/2011 (Figure 1f), and as small as 5 K in 2008/2009 (Figure 1e). The latter was attributed by *Gu et al.* [2013] to weaker summer easterly jets during that year, noting that the W4 QTDW component (not shown) was unusually dominant that year. The southern summer W3 QTDW events manifest as a single large peak during each season, with durations on the order of 20–40 days, depending upon the individual year.

Table 1. QTDW Events Utilized in the Study[a]

Season	QTDW Peak Day
2003/2004	45
2004/2005	55
2005/2006	47
2006/2007	53
2008/2009	55
2010/2011	50

[a]Day 0 corresponds to 1 December of the earlier year.

We now explore changes to the background zonal winds that may be driven by the W3 QTDW using TIDI zonal wind observations from 85 km. The TIDI background zonal winds at 85 km as a function of latitude and time obtained from the aforementioned averaging process are shown in Figure 2. The days of peak W3 QTDW amplitudes identified using SABER (Table 1) are again marked by dashed red lines. It is apparent that for all years examined, background zonal winds equatorward of about 30° in both hemispheres become more westward in the days following the peak W3 QTDW amplitudes. The magnitude and duration of this westward shift vary from year to year, although the low-latitude background zonal winds of all years are characterized by an eastward to westward shift around the time of the W3 QTDW peak, consistent with westward forcing imposed on the zonal mean zonal winds by the QTDW [*Lieberman*, 1999; *Chang et al.*, 2011a]. Regions of
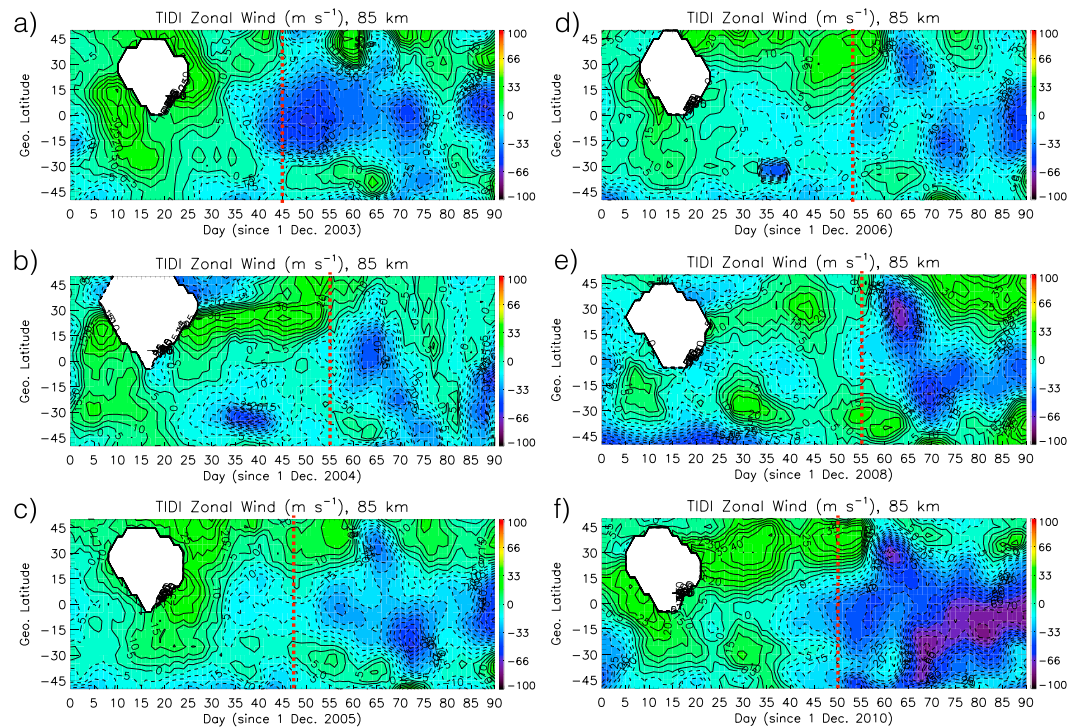
Figure 2. Same as Figure 1 but for background zonal winds in TIDI at 85 km. Contour intervals of 5 m s^{-1}.

eastward winds also appear poleward of 30° in the days after the W3 QTDW peak; however, it is unclear if this corresponds to changes in the zonal mean zonal winds, or SW2, which also has zonal wind amplitude peaks in the midlatitudes.

We further isolate rapid changes in the aforementioned 6 day averaged background zonal winds by removing the background zonal winds calculated using a 60 day sliding window, the latter of which allows for unambiguous resolution of the zonal mean zonal winds on a seasonal scale. The background zonal wind anomalies that result from the difference between the 6 day and 60 day mean background winds represent variability with time scales between 6 and 60 days. This allows the retention of QTDW-related variability, since the duration of an average QTDW event is on the order of 40 days, as seen later in Figure 6. These can be utilized to further elucidate potential QTDW-related changes to the background zonal winds at 85 km, with time scales shorter than seasonal. It should be noted that these anomalies include both short-term fluctuations in the zonal mean zonal winds, as well as contributions from SW2 at the local time of sampling. The latter will be located mainly in the midlatitude region where SW2 zonal wind amplitudes maximize. DW1 residuals from missing data points will also be present but can be expected to vary randomly from year to year.

The background zonal wind anomalies are shown in Figure 3. Some consistent features are again apparent in the background zonal wind anomalies during the days surrounding a QTDW event. During all of the years examined, background zonal wind anomalies in the Northern Hemisphere show a pronounced westward shift within about 5 days of the peak QTDW amplitudes, centered at latitudes varying between 10 and 30°N. The magnitudes of these westward anomalies range from about 30 to 80 m s^{-1}, with the largest values appearing in 2008/2009 (Figure 3e) and 2010/2011 (Figure 3f), despite the fact that the W3 QTDW amplitudes at 85 km in 2008/2009 (Figure 1e) were the smallest of all the years examined. The magnitudes of these QTDW-related wind anomalies are within the range of 10–100 m s^{-1} found by previous studies [*Plumb et al.*, 1987; *Fritts et al.*, 1999; *Lieberman*, 1999; *Chang et al.*, 2011a, and references therein]. The duration of these Northern Hemisphere westward anomalies is roughly 15–20 days. These westward anomalies may also extend across the equator into the Southern Hemisphere during some years, particularly during 2003/2004 (Figure 3a), 2004/2005 (Figure 3b), and 2010/2011 (Figure 3f).
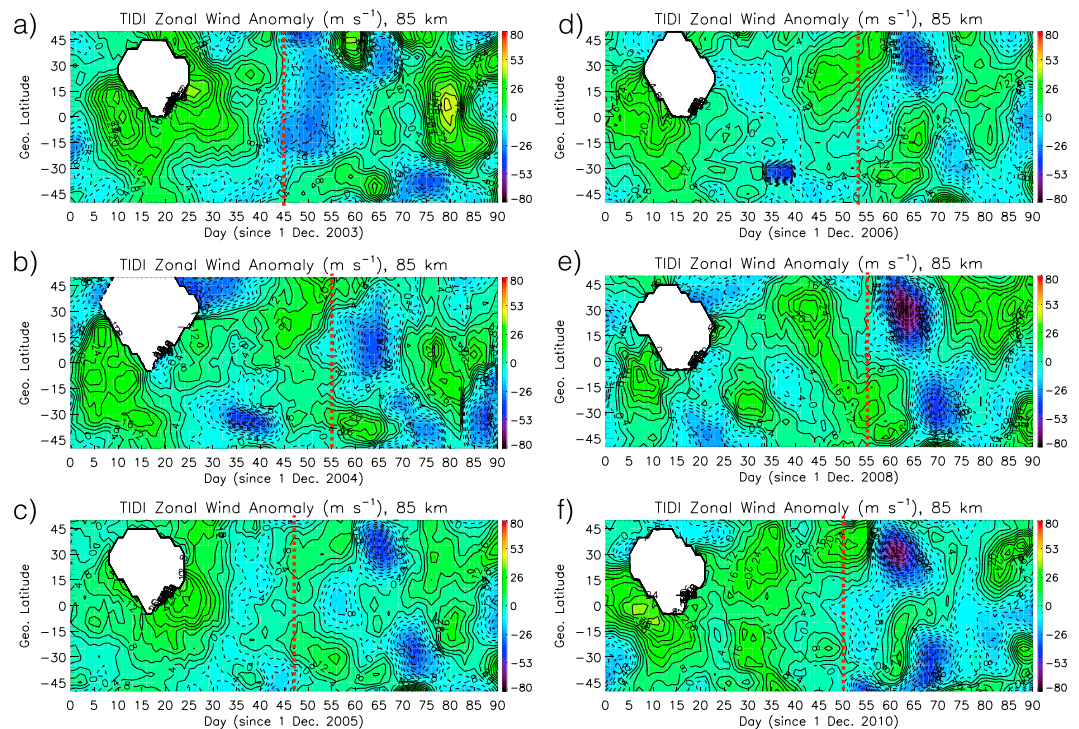
Figure 3. Same as Figure 1 but for background zonal wind anomalies in TIDI at 85 km. Contour intervals of 4 m s^{-1}.

The timing of these westward anomalies again suggests a connection to westward forcing imposed on the zonal mean zonal winds by the W3 QTDW dissipation. The location of the westward anomaly in the Northern Hemisphere at 85 km is consistent with the propagation of the W3 QTDW from the westward jet in the summer midlatitude upper stratosphere/lower mesosphere, across the equator into the northern mesopause region. This is consistent with the structure of the W3 QTDW waveguide determined in past modeling studies [*Liu et al.*, 2004; *Chang et al.*, 2011a; *Yue et al.*, 2012a].

A secondary westward anomaly also occurs in the southern midlatitudes centered between 30 and 40°S, roughly 10–20 days after the QTDW peak during all years examined. This is preceded by an eastward anomaly in the same latitudinal region. The eastward anomaly may potentially be due to forcing from gravity waves filtered by westward zonal mean zonal winds driven by the QTDW at lower altitudes, as was seen in simulations by *Chang et al.* [2011a]. However, contributions from SW2 also cannot be excluded, due to the proximity to the SW2 zonal wind amplitude peaks near 50°S.

Although it is apparent that the QTDW is acting to drive background wind changes at 85 km, this altitude is still located below the turbopause at roughly 100 km. As such, the atmosphere in this region is already well mixed by strong eddy diffusion. To examine whether QTDW-related background wind changes are apparent at the turbopause, we display in Figure 4 the background zonal wind anomalies at 100 km. Although considerable interannual variability is apparent, it can be seen that for all the years examined, the background zonal winds at 100 km show a distinctive switch from mostly eastward to westward in the days following the peak QTDW amplitudes, mainly in the northern low latitudes and equatorial region. The time delay between the day of peak QTDW amplitudes and the background wind reversal ranges from as short as 12 days in 2004/2005 (Figure 4b) to as long as 20 days in 2010/2011 (Figure 4f). The duration of this time delay may be related to the time required for QTDW-related background wind forcing to extend further upward from the region of peak amplitudes around 85 km. Additionally, the initial eastward background winds at 100 km may be related to forcing from gravity waves filtered by the background winds at lower altitudes that are subjected to westward QTDW forcing at earlier times.

From the preceding analysis of W3 QTDW amplitudes using SABER and concurrent background zonal winds from TIDI, it is apparent that the QTDW is indeed inducing significant changes to the background zonal winds in the MLT region as high up as the turbopause, with direction and spatial structure consistent with
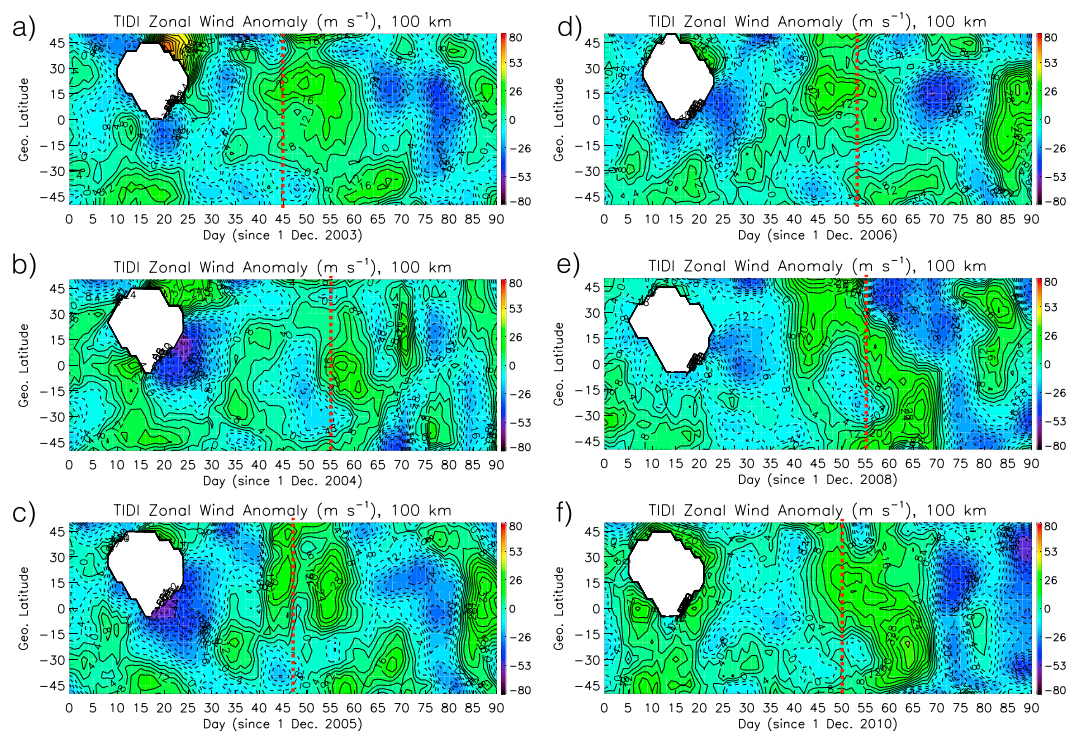
Figure 4. Same as Figure 1 but for background zonal wind anomalies in TIDI at 100 km. Contour intervals of 4 m s^{-1}.

past numerical experiments. We now consider changes occurring in the thermosphere and ionosphere, to determine whether evidence exists for large-scale mixing related to QTDW-induced MLT wind changes.

Figure 5 shows the zonal mean values at each magnetic latitude of ionospheric total electron content (TEC) determined from GIM at 16 h local time for all six QTDW events examined. This local time corresponds to the largest daytime values of the equatorial ionization anomalies (EIAs). As TEC is influenced by both changes related to lower atmospheric effects, as well as solar and geomagnetic effects, the daily $F_{10.7}$ solar radio flux (thin dashed red line) and geomagnetic Kp (solid red line) indices are also superimposed. Values of Kp in excess of five represent geomagnetic storm conditions, which are present during all years except 2005/2006, 2008/2009, and 2010/2011. Baseline values of $F_{10.7}$ vary from around 68 sfu (solar flux units or 10^{-22} W m^{-2} Hz^{-1}) during the 2008/2009 solar minimum to as high as 110 sfu in the 2003/2004 postsolar maximum period. Sporadic $F_{10.7}$ spikes in the range of 20–40 sfu of 5–10 days in duration are also apparent during all seasons except 2008/2009 and may correspond to solar flares. The day of peak QTDW amplitudes is again identified for each year by the vertical dashed red line. Decreases in TEC within ± 5 days of the peak MLT QTDW amplitudes can be seen for all 6 years examined and will now be examined individually to consider possible influences from solar and geomagnetic effects.

Short periods of storm conditions and elevated $F_{10.7}$ are present within 10 days of the SABER determined QTDW peak in 2003/2004 (Figure 5a) and 2004/2005 (Figure 5b), and geomagnetic contributions to TEC variability during the QTDW events of these years cannot be discounted. Solar and geomagnetic activity during the other years are generally low within the 10 days surrounding the QTDW peak amplitudes, particularly during 2008/2009 (Figure 5e) and 2010/2011 (Figure 5f), with Kp values around 3 or less, and $F_{10.7}$ fluctuations of 5 sfu or less. We first consider TEC variations during the relatively quiet periods of these 2 years.

From Figures 5e and 5f, a prominent TEC decrease is evident at low latitudes roughly centered on the day of peak QTDW amplitudes at 85 km, also marked with a vertical dashed red line. The decrease is on the order of 8–9 TECU (total electron content unit; 1 TECU = 10^{16} el m^{-2}) for these 2 years, compared to values immediate preceding the decrease. A similar TEC decrease centered approximately 2 days before the QTDW peak amplitudes can also be resolved in 2005/2006 (Figure 5c). Some changes about 10 days after the QTDW peak amplitudes may be affected by elevated solar and geomagnetic activity. Similar TEC decreases around
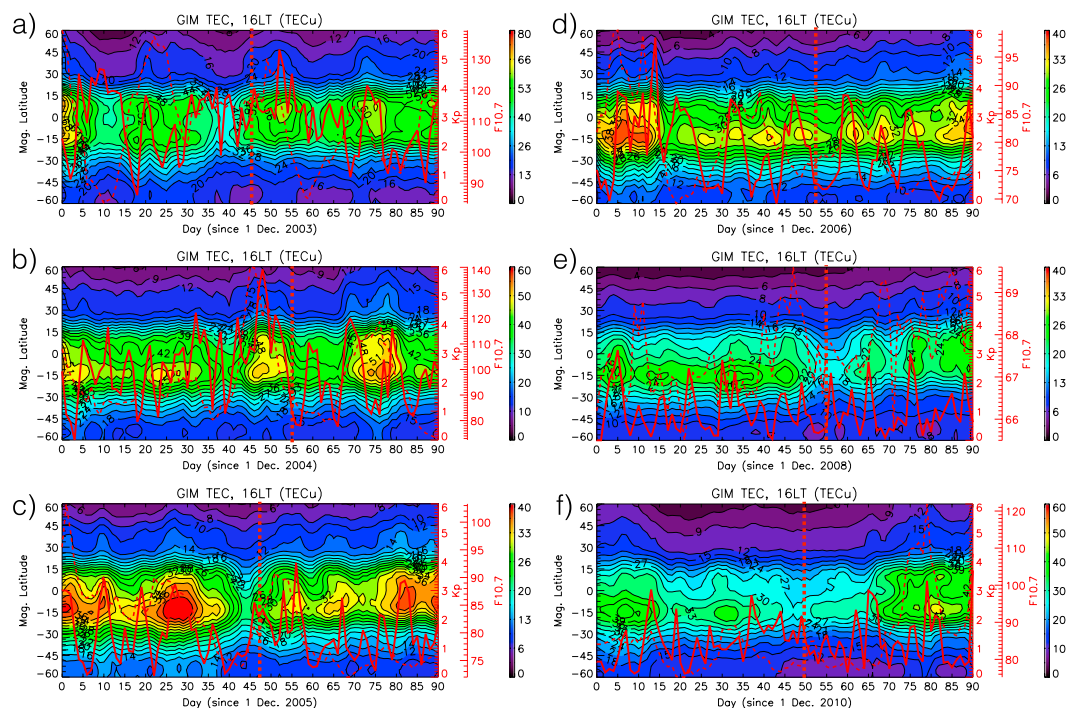
Figure 5. Same as Figure 1 but for zonal mean GIM TECs at 16 LT. Superimposed solid red line denotes daily Kp index, thin dashed red line denotes daily $F_{10.7}$ index. Note the varying scales for $F_{10.7}$ from year to year.

the day of QTDW peak amplitudes can also be seen in 2003/2004 (Figure 5a) and 2004/2005 (Figure 5b), although elevated TEC levels potentially related to storms are seen in the 10 days after and before the QTDW peak day, respectively. Given the 10 day gap between the QTDW peak day and the geomagnetic storms during these 2 years, the decreased TEC levels around the QTDW peak days are unlikely to be due to negative storm effects.

Variations in TEC related to the QTDW are difficult to distinguish from geomagnetically driven disturbances in 2006/2007 (Figure 5d), due to repeated spikes in $F_{10.7}$ and Kp surrounding the QTDW peak day. Nonetheless, we can conclude that there is an unambiguous QTDW signature in TEC for those cases that are free from significant solar and geomagnetic forcing.

To further highlight the relationship between QTDW-related changes in the MLT and in the ionosphere, we present averages over all 6 years around the period of peak QTDW amplitude for SABER W3 QTDW temperature amplitude at 85 km (Figure 6a), TIDI background zonal winds anomalies at 85 km (Figure 6b), TIDI background zonal wind anomalies at 100 km (Figure 6c), and GIM zonal mean TEC anomaly at 16 h local time. Since the interannual averaging is centered on the day of maximum QTDW amplitudes, non-QTDW-related sub-60 day variability will be suppressed.

From the multiyear averaged SABER W3 QTDW temperature amplitudes at 85 km shown in Figure 6a, we can see more clearly the latitudinal structure of the W3 QTDW in the MLT. The W3 QTDW expands from the southern midlatitudes for a time of about 25 days, eventually evolving into the distinct 3,0 Rossby-gravity normal mode structure on the QTDW peak amplitude day (Day 0). This is then followed by a more rapid decrease in amplitude over the course of about 10 days in the southern subtropics and 15 days in the southern midlatitudes. *Chang et al.* [2011a] attributed this behavior to variations in the QTDW waveguide via QTDW-induced forcing on the zonal mean zonal winds.

The background zonal wind anomalies are again obtained by suppressing seasonal changes in the zonal mean zonal winds through removal of the daily 60 day mean values from the daily 6 day averaged TIDI background zonal winds and then averaging over all years. These multiyear averaged anomalies at 85 km are shown in Figure 6b. The westward shifts in equatorial and northern low- to middle-latitude background zonal winds are now more visible in the days following the MLT QTDW peak amplitude. These persist for up
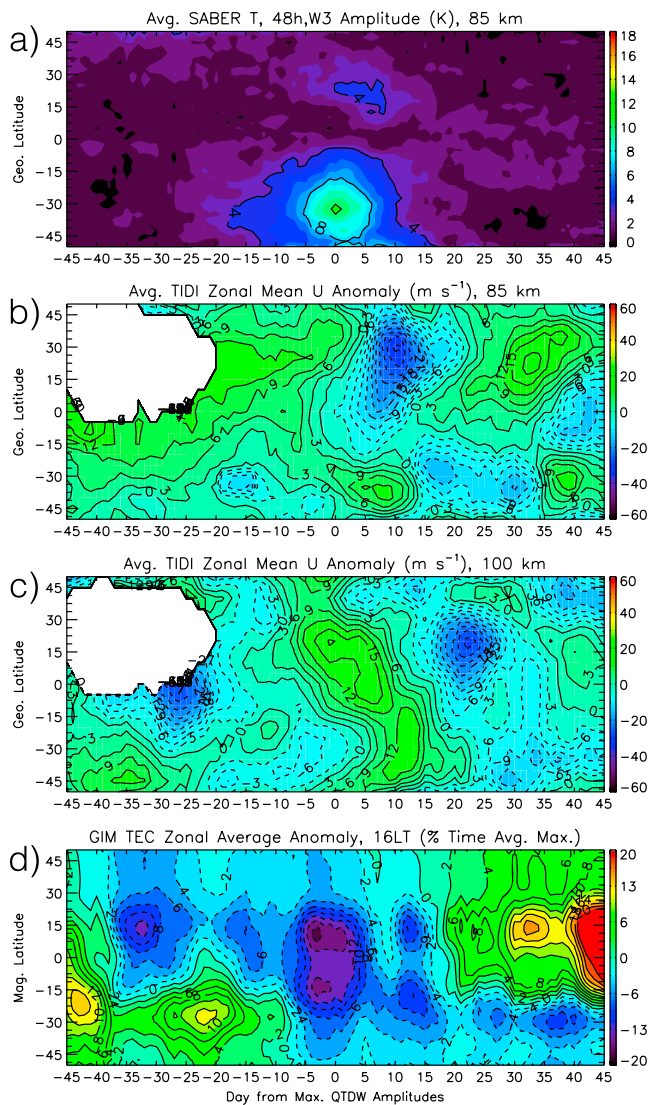
Figure 6. Latitude/time plots of multiyear averages centered on day of peak W3 QTDW amplitudes (Day 0) for (a) W3 QTDW amplitudes in SABER temperatures at 85 km, (b) TIDI background zonal winds anomalies at 85 km, (c) TIDI background zonal wind anomalies at 100 km, and (d) anomalies of zonal mean GIM TECs at 16 LT.

to 20 days with values up to 27 m s^{-1}. The eastward enhancements in the southern midlatitudes are also evident and seem to persist for about 10 days on average. The magnitudes of these background wind changes are considerably larger than the aforementioned TIDI wind measurement uncertainties of 2 m s^{-1} and cannot be attributed to random noise [*Yue et al.*, 2013b]. The presence of both of these features in the anomalies strongly suggests that they are related to the QTDW, rather than the normal seasonal variation, and are also consistent with the spatial structure of the QTDW waveguide and the secondary eastward forcing effects of filtered gravity waves.

The multiyear averaged background wind anomalies at turbopause heights of 100 km are shown in Figure 6c. The background wind anomalies in the northern low to middle latitudes show a transition from slightly westward to eastward then back to strong westward. The latter eastward to westward reversal occurs about 10 days following the day of MLT QTDW peak amplitude and persists for about 20 days. The presence of the average eastward to westward transition in the days following the QTDW event across the multiple years examined again suggests that it is a robust feature, demonstrating that QTDW forcing effects on the background winds can extend up to at least turbopause heights. The eastward anomalies centered
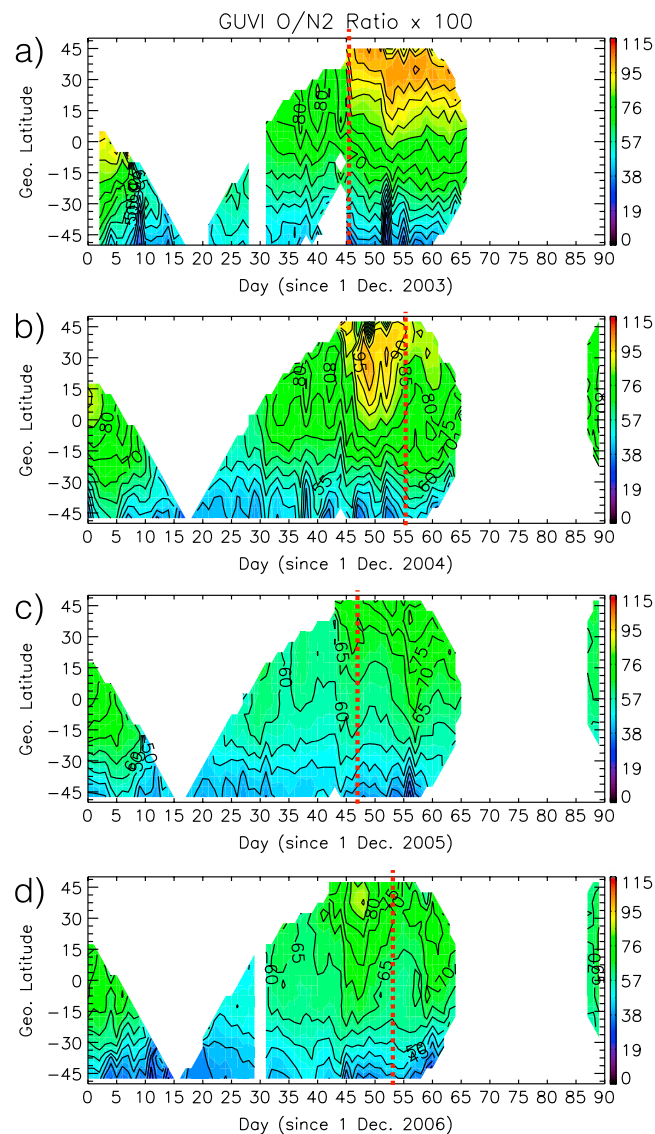
Figure 7. GUVI ΣO/N2 ratio (multiplied by 100) as a function of geographic latitude and time for southern summers during (a) 2003/2004, (b) 2004/2005, (c) 2005/2006, and (d) 2006/2007. Day 0 corresponds to 1 December, day of peak QTDW amplitudes determined by SABER marked by dashed red line. Contour interval of 5.

around Day 0 may again be related to eastward forcing effects from gravity waves filtered by the westward background winds at lower levels with earlier onset times, as seen in Figure 6b.

In Figure 6d, we plot the multiyear average of GIM TEC anomalies zonally averaged at 16 LT. Because we are only interested in the latitudinal-temporal variability, we put the TEC anomalies on the same magnitude scale by normalizing the values from each of the 6 years to the maximum low-latitude TEC value averaged over the 90 day period surrounding each QTDW event (hereafter referred to as the time-averaged maximum TEC). Normalizing all anomalies to a single value ensures that the latitudinal structure of the TECs is retained, while suppressing variations in TEC due to the solar cycle. The normalized TECs from all 6 years were then averaged about the day of peak QTDW amplitudes, and the anomaly was determined by removing the 90 day mean of the averaged normalized TECs from each latitude. The multiyear average also ensures that the effect of geomagnetic activity, which is pseudorandom in this context, is suppressed.

Figure 6d shows TEC decreases at EIA latitudes in both hemispheres of up to 16% of the time-averaged maximum TEC in the roughly 15 days surrounding the peak MLT QTDW amplitudes. This is in agreement with the model simulated TEC decrease of ∼ 20% by *Yue and Wang* [2014]. A secondary decrease is also resolved
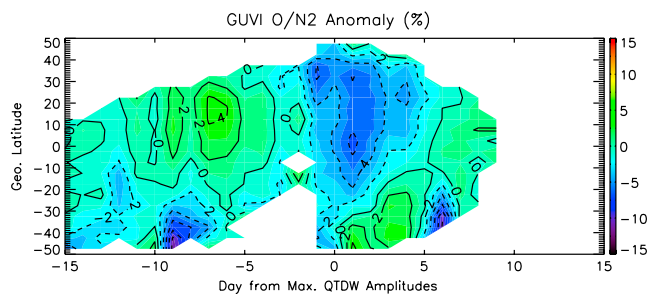
Figure 8. GUVI $\Sigma O/N2$ ratio anomaly (%) averaged from 2003/2004 to 2006/2007, centered on day of peak W3 QTDW amplitudes (Day 0). Contour interval of 2%.

at EIA latitudes from Days 10 to 15, with smaller decreases in the southern (northern) EIA regions present in the days following (preceding) the peak MLT QTDW amplitudes. Although the current sample set of 6 years is too small for additional statistical analysis, it does provide strong evidence of an anticorrelation between QTDW amplitudes in the MLT and TECs in the ionospheric EIA regions.

We next consider the potential role of mixing resulting from QTDW-induced general circulation changes and how it might cause the TEC decreases. Westward zonal forcing by the QTDW on zonal mean zonal winds of the equatorial lower thermosphere (similar to that resolved by the TIDI anomalies in Figures 6b and 6c) can be expected to produce poleward flow in both hemispheres through Coriolis deflection. The induced mixing increases molecular nitrogen mixing ratio and decreases the atomic oxygen mixing ratio in the thermosphere, resulting in increased plasma loss rates [*Yamazaki and Richmond*, 2013; *Yue and Wang*, 2014]. This composition change should be manifested in the thermosphere $\Sigma O/N_2$ ratios.

Figure 7 shows the $\Sigma O/N_2$ ratio observed in GUVI limb observations during four of the six previously shown QTDW events before 2008, with the day of peak QTDW amplitudes in the MLT again marked by the dashed red lines. Despite the more limited coverage, a few common features can still be seen across all the years shown. During time scales on the order of the observational period, the $\Sigma O/N_2$ ratio is generally largest in the Northern Hemisphere and smallest in the Southern Hemisphere. This distribution is consistent with seasonal upwelling in the summer hemisphere acting to increase molecular species concentrations (thus decreasing $\Sigma O/N_2$), and seasonal downwelling in the winter hemisphere acting to enhance atomic oxygen concentrations [*Mayr and Volland*, 1972; *Qian et al.*, 2009].

Decreases in O/N_2 are observed for a duration on the order of about 5–10 days around the time of peak QTDW amplitudes for each year examined. In order to see this decrease in $\Sigma O/N_2$ more clearly, we compute $\Sigma O/N_2$ anomalies using the same approach as that for TEC. The solar cycle effect in the ratios from 2003 to 2007 is first removed via normalization to the mean value. The normalized $\Sigma O/N_2$ from all 4 years at each latitude is then averaged about the day of peak QTDW amplitudes, and the anomaly was determined by removing the 90 day mean from each latitude. The multiyear average of $\Sigma O/N_2$ anomalies in the 30 days surrounding the peak QTDW day is shown in Figure 8. Note that the time span has been shortened from previous plots to account for the more limited GUVI observations.

It is apparent that decreases in $\Sigma O/N_2$ of up to 6% are seen in the 5 days following the peak MLT QTDW amplitudes; they also seem to begin as early as about 5 days before. The largest decreases are centered about the northern (winter) tropics, extending as far poleward as the northern midlatitudes. As the TIDI winds at 85 km and 100 km show QTDW-related changes on global background winds, we can conclude that westward mean wind forcing from QTDW dissipation and eastward anomalies potentially related to filtered gravity wave effects can drive circulation changes up to turbopause altitudes. The modeling results of *Yue and Wang* [2014] clearly showed that these QTDW-induced global circulation changes in the lower thermosphere from 100 to 150 km can have an effect on thermospheric composition above 100 km.

These compositional effects, along with the previously shown changes in MLT background zonal winds from TIDI, as well as the decreases in low-latitude TEC, provide strong evidence that the W3 QTDW event in the MLT is acting to reduce ionospheric TEC through composition changes caused by increased mixing from the QTDW-induced general circulation changes.

4. Discussion

The preceding results show interannually recurrent features occurring in the MLT background zonal winds, ionospheric TECs, and $\Sigma O/N_2$ ratios around the time of W3 QTDW events during the January postsolstice period. The MLT background zonal wind changes are consistent with those resolved by previous simulations of the W3 QTDW. They result from westward mean wind forcing produced by the dissipating westward propagating wave, which appears initially in the mesosphere and eventually expands upward to turbopause altitudes. Background zonal winds at the turbopause also show an initial eastward shift at the same time as the maximum QTDW amplitudes, which may be related to gravity waves filtered by the more westward winds below [*Chang et al.*, 2011a; *Yue et al.*, 2012a]. The changes resolved in the ionospheric TECs and $\Sigma O/N_2$ ratios are consistent with features identified by *Yamazaki and Richmond* [2013] in the context of the migrating atmospheric tides, and by *Yue and Wang* [2014] for the case of the QTDW. Namely, we have found changes to the thermosphere general circulation in the presence of strong westward wave forcing in the MLT region and decreased O/N_2 ratios, potentially due to increased mixing from the subsequently induced meridional circulation.

Although we cannot explicitly exclude eddy mixing from altered gravity wave diffusion as an additional mechanism from our observations alone, we note that the numerical experiments of *Yamazaki and Richmond* [2013] found that the induced meridional circulation from the dissipating migrating tides played a much greater role in driving thermosphere composition changes, compared to induced changes in vertical diffusion and eddy diffusivity. Although *Yamazaki and Richmond* [2013] focused on the effects of the westward propagating migrating tides, it is likely that a similar relation holds in the case of the W3 QTDW. The TEC changes resolved in that study started with a small increase due to enhancement of the equatorial fountain mechanism by the imposition of the migrating semidiurnal tide (SW2), which transitioned to a much larger decrease within about 5 days from the onset of forcing. This time scale is well within the 20–40 day durations of the W3 QTDW events examined in this study, which may in fact result in faster TEC depletion if the equatorial fountain is not enhanced.

Yue and Wang [2014] used the thermosphere-ionosphere-mesosphere electrodynamics general circulation model to study the effect of QTDW dissipation on thermospheric composition (O/N_2) and ionospheric electron density during solar minimum. Applying QTDW forcing at the model's lower boundary and comparing the results to a model run without QTDW forcing, they found that the westward propagating QTDW deposits momentum in the lower thermosphere that enhances the westward mean wind and drives poleward meridional circulation. This increases the mixing in the lower thermosphere and results in a decrease of the O mixing ratio and an increase of the N_2 and O_2 mixing ratios in the upper thermosphere by molecular diffusion. As a result, the O/N_2 ratio near the ionospheric *F* region is reduced, leading to a depletion in the background *F* region electron density and TEC at low and middle latitudes. This paper presents direct observational evidence of such a coupling process between the QTDW and the thermosphere/ionosphere system.

It is also interesting to note that other transient wave-driven events in the middle atmosphere such as stratospheric sudden warmings can also drive changes in MLT background winds on similar time scales and could thus conceivably affect the thermosphere and ionosphere in an analogous manner [*Liu and Roble*, 2002; *Chandran et al.*, 2013].

Although the W3 QTDW can produce considerable westward forcing on the MLT mean winds, it is also interesting to note that the migrating diurnal tide is known to show significant amplitude decreases in the MLT region during a W3 QTDW event due to the altered background winds, as well as nonlinear advection [*Chang et al.*, 2011a, and references therein]. The general circulation changes driven by the dissipating migrating diurnal tide were found by *Yamazaki and Richmond* [2013] to also play an important role in driving thermosphere and ionosphere changes through increased tidal mixing, as mentioned previously. Taken alone, the suppression of migrating diurnal tidal amplitudes by the W3 QTDW ought to also result in a suppression of tidal mixing. Since our observational results still show evidence for enhanced mixing during W3 QTDW events, this suggests that the "planetary wave mixing" induced by the W3 QTDW is sufficiently large to compensate for the reduction in tidal mixing. Changes to the *E* region dynamo due to the altered tides, however, are a separate issue that must be addressed in future studies.

5. Conclusions

We have presented observational evidence from six case studies of W3 QTDW events that important changes occur in both the dynamics of the MLT as well as ionospheric TECs, and thermosphere composition. MLT background zonal winds from TIDI show both large westward anomalies around the time of the W3 QTDW event identified in SABER temperatures that are consistent with forcing by the dissipating westward propagating QTDW, as well as eastward anomalies that may be related to filtered gravity wave effects [*Chang et al.*, 2011a]. GIM TEC data show decreases during this time, especially in the EIA region. These are accompanied by decreases in GUVI $\Sigma O/N_2$ ratios, which can be expected to reduce ionospheric TECs by chemical processes [*Fuller-Rowell*, 1998; *Qian et al.*, 2009; *Lean et al.*, 2011; *Yamazaki and Richmond*, 2013]. Taken together, the observations provide strong evidence that the general circulation changes caused by the dissipating W3 QTDW in the lower thermosphere can drive additional changes in the ionosphere and thermosphere through composition changes induced through enhanced mixing. The "planetary wave mixing" identified in our study has the potential to drive transient thermospheric and ionospheric variability during strong planetary wave events in the MLT region. In the future, additional studies using ground-based measurements over longer periods of time will be helpful in augmenting the 6 years examined using our global-scale data sets.

Appendix A: TIDI DW1 Residual Analysis

Figure A1a shows the local time distributions of TIDI observations on 9 January 2004, which are grouped into two distinct tracks for the cold side of the spacecraft (facing away from the Sun) and warm side samplings. During this particular day, the cold side (warm side) track covers all latitudes within the Southern (Northern) Hemisphere, with the sampled local times being more similar in the Southern (Northern) Hemisphere, compared to the latitudes near the turning point in the Northern (Southern) Hemisphere. This sampling pattern is identical from day to day, with changes reflecting the 12 min per day TIMED local time precession rate. Additionally, changes to the hemisphere fully covered by the cold and warm side take place when the TIMED spacecraft undergoes a yaw maneuver every 63 days in order to keep the cold side facing away from the Sun. For additional discussion of TIDI sampling, we refer the reader to *Wu et al.* [2006].

In the TIDI background zonal wind analysis employed in this study, we are particularly concerned with the potential for aliasing from the migrating diurnal tide (DW1), especially around the peak in DW1 zonal wind amplitudes near $\pm20°$ latitude from the diurnal 1,1 Hough mode [*Wu et al.*, 2006]. DW1 can be suppressed by averaging values at the same latitude but separated 12 h in local time. Incomplete suppression of DW1 in this study can therefore arise from the following possibilities:

1. The TIMED spacecraft orbit is not perfectly polar. Thus, local time separation between points at the same latitude on ascending and descending tracks is not always 12 h, especially near the turning points between 45 and 60° latitude.
2. Data gaps along the TIDI sampling tracks may result in incomplete cancelation.

We have tested three zonal and time averaging methods for calculating the TIDI background winds. Method 1 utilizes all available TIDI data points, as shown in Figure A1a, including those near the turning points. Similar to [*Wu et al.*, 2006], the two other methods involve the removal of data points in the hemisphere of the turning points ether poleward of the equator (Method 2, not shown), or poleward of 15° in the turning point hemisphere (Method 3, Figure A1b). By removing data points in the hemisphere of the turning point, we can ensure a local time separation of roughly 12 h is maintained between sample points along each track in the midlatitudes.

We quantify the level of potential DW1 aliasing resulting from these three averaging methods using the following methodology: in-phase ($I = \cos(\Omega t_{LT})$, $\Omega = \frac{2\pi}{24}$ h^{-1}) and quadrature ($Q = \sin(\Omega t_{LT})$) DW1 test signals of unit amplitude are sampled using the same space/time distribution as the TIDI observations and averaged in the same manner as that used for the background zonal winds described in section 2.2, yielding averaged residuals $\bar{I}$ and $\bar{Q}$. The magnitude of the averaged in-phase and quadrature residuals ($M = \sqrt{\bar{I}^2 + \bar{Q}^2}$, hereafter referred to as the residual magnitude) reflects the level of potential aliasing from DW1 into the background zonal winds, with a value of $M = 1$ corresponding to the strong possibility of constructive or destructive interference from the superposition of the full amplitude of the tide upon the zonal
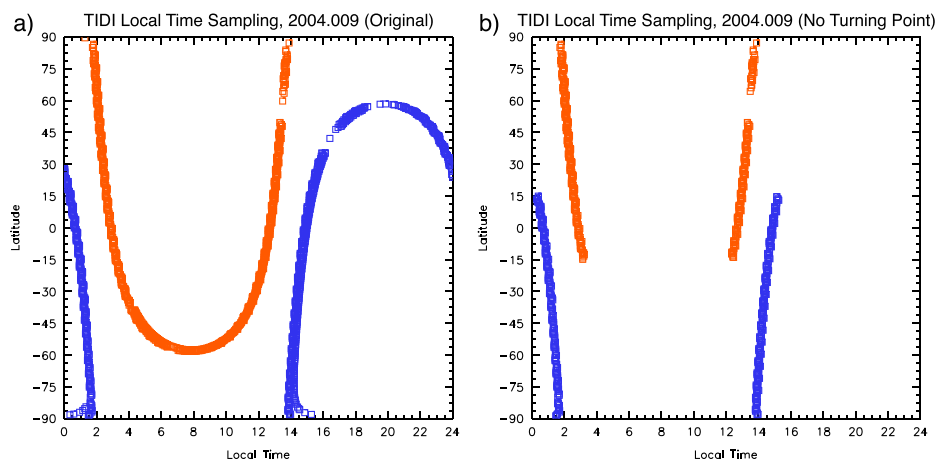
Figure A1. Local time distribution as a function of latitude for TIDI observations on 9 January 2004. Red (blue) points correspond to warm (cold) side track. (a) Original samples (Method 1) and (b) samples used in analysis with data points removed poleward of 15° in hemisphere of turning points (Method 3).
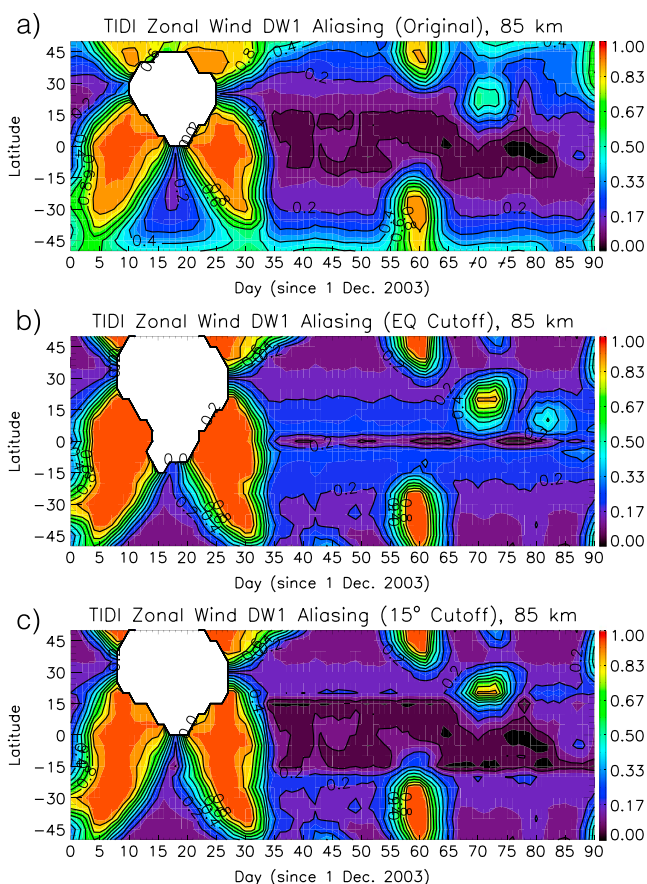

Figure A2. Magnitude of potential aliasing from DW1 into TIDI background winds computed using (a) all data points (Method 1), (b) removal of all data points in hemisphere of turning point (Method 2), and (c) removal of all data points poleward of 15° in hemisphere of turning point (Method 3). Results correspond to 2003/2004.

mean zonal winds. A value of $M = 0$ corresponds to full cancelation of DW1 resulting from sampling intervals of 12 h, while intermediate values of M correspond to varying levels of incomplete DW1 suppression. The use of in-phase and quadrature terms in this method allows us to account for the possibility that the tidal phase can vary relative to the local times sampled by TIDI.

The results of this residual magnitude analysis are shown in Figure A2 for the three aforementioned averaging methods in 2003/2004. Similar results were also found for the other seasons examined in this study. For all three methods, a high potential for aliasing of the background zonal winds with DW1 exists over the first 35 days of the observational period due to the reduced number of TIDI observations during this time, but is reduced in the following time period.

During this time, the three averaging methods show distinct differences in terms of the residual magnitudes in the low latitudes. In particular, Method 1 using all available TIDI data points (Figure A2a) has considerably smaller residual magnitudes near the zonal wind amplitude peaks of the diurnal 1,1 Hough mode at $\pm 20°$ latitude, compared to the two other methods that removed data points near the turning points (Figures A2b and A2c). Although not removing data points near the turning point results in elevated residual magnitudes in the midlatitudes near the turning points with Method 1, actual aliasing from DW1 in this region should be minor since the zonal wind amplitudes of the upward propagating DW1 Hough modes are known to be largest in the low latitudes. We therefore select Method 1 for calculation of the background zonal winds utilized in this study.

References

Chandran, A., R. R. Garcia, R. L. Collins, and L. C. Chang (2013), Secondary planetary waves in the middle and upper atmosphere following the stratospheric sudden warming event of January 2012, *Geophys. Res. Lett.*, *40*, 1861–1867, doi:10.1002/grl.50373.

Chang, L. C., S. E. Palo, and H.-L. Liu (2011a), Short-term variability in the migrating diurnal tide caused by interactions with the quasi 2 day wave, *J. Geophys. Res.*, *116*, D12112, doi:10.1029/2010JD014996.

Chang, L. C., J.-Y. Liu, and S. E. Palo (2011b), Propagating planetary wave coupling in SABER MLT temperatures and GPS TEC during the 2005/2006 austral summer, *J. Geophys. Res.*, *116*, A10324, doi:10.1029/2011JA016687.

Chang, L. C., C.-H. Lin, J.-Y. Liu, N. Balan, J. Yue, and J.-T. Lin (2013a), Seasonal and local time variation of ionospheric migrating tides in 2007–2011 FORMOSAT-3/COSMIC and TIE-GCM total electron content, *J. Geophys. Res. Space Physics*, *118*, 2545–2564, doi:10.1002/jgra.50268.

Chang, L. C., C.-H. Lin, J. Yue, J.-Y. Liu, and J.-T. Lin (2013b), Stationary planetary wave and nonmigrating tidal signatures in ionospheric wave 3 and wave 4 variations in 2007–2011 FORMOSAT-3/COSMIC observations, *J. Geophys. Res. Space Physics*, *118*, 6651–6665, doi:10.1002/jgra.50583.

Chen, P.-R. (1992), Two-day oscillation of the equatorial ionization anomaly, *J. Geophys. Res.*, *97*(A5), 6343–6357, doi:10.1029/91JA02445.

Christensen, A. B., et al. (2003), Initial observations with the Global Ultraviolet Imager (GUVI) in the NASA TIMED satellite mission, *J. Geophys. Res.*, *108*(A12), 1451, doi:10.1029/2003JA009918.

Dow, J. M., R. E. Neilan, and C. Rizos (2009), The international GNSS service in a changing landscape of Global Navigation Satellite Systems, *J. Geod.*, *83*, 191–198, doi:10.1007/s00190-008-0300-3.

England, S. L., T. J. Immel, E. Sagawa, S. B. Henderson, M. E. Hagan, S. B. Mende, H. U. Frey, C. M. Swenson, and L. J. Paxton (2006), Effect of atmospheric tides on the morphology of the quiet time, postsunset equatorial ionospheric anomaly, *J. Geophys. Res.*, *111*, A10S19, doi:10.1029/2006JA011795.

Forbes, J. M., R. G. Roble, and C. G. Fesen (1993), Acceleration, heating, and compositional mixing of the thermosphere due to upward propagating tides, *J. Geophys. Res.*, *98*(A1), 311–321, doi:10.1029/92JA00442.

Forbes, J. M., X. Zhang, S. Palo, J. Russell, C. J. Mertens, and M. Mlynczak (2008), Tidal variability in the ionospheric dynamo region, *J. Geophys. Res.*, *113*, A02310, doi:10.1029/2007JA012737.

Forbes, J. M., S. L. Bruinsma, X. Zhang, and J. Oberheide (2009), Surface-exosphere coupling due to thermal tides, *Geophys. Res. Lett.*, *36*, L15812, doi:10.1029/2009GL038748.

Fritts, D. C., J. R. Isler, R. S. Lieberman, M. D. Burrage, D. R. Marsh, T. Nakamura, T. Tsuda, R. A. Vincent, and I. M. Reid (1999), Two-day wave structure and mean flow interactions observed by radar and High Resolution Doppler Imager, *J. Geophys. Res.*, *104*, 3953–3969.

Fuller-Rowell, T. J. (1998), The "thermospheric spoon": A mechanism for the semiannual density variation, *J. Geophys. Res.*, *103*, 3951–3956.

Gu, S.-Y., T. Li, X. Dou, Q. Wu, M. G. Mlynczak, and J. M. Russell (2013), Observations of quasi-two-day wave by TIMED/SABER and TIMED/TIDI, *J. Geophys. Res. Atmos.*, *118*, 1624–1639, doi:10.1002/jgrd.50191.

Killeen, T. L., Q. Wu, S. C. Solomon, D. A. Ortland, W. R. Skinner, R. J. Niciejewski, and D. A. Gell (2006), TIMED Doppler interferometer: Overview and recent results, *J. Geophys. Res.*, *111*, A10S01, doi:10.1029/2005JA011484.

Lean, J. L., R. R. Meier, J. M. Picone, and J. T. Emmert (2011), Ionospheric total electron content: Global and hemispheric climatology, *J. Geophys. Res.*, *116*, A10318, doi:10.1029/2011JA016567.

Lieberman, R. S. (1999), Eliassen-Palm fluxes of the 2-day wave, *J. Atmos. Sci.*, *56*, 2846–2861, [Corrigendum, J. Atmos. Sci., 59, 2625–2627, 2002].

Limpasuvan, V., and D. L. Wu (2009), Anomalous two-day wave behavior during the 2006 austral summer, *Geophys. Res. Lett.*, *36*, L04807, doi:10.1029/2008GL036387.

Liu, H.-L., and R. G. Roble (2002), A study of a self-generated stratospheric sudden warming and its mesospheric-lower thermospheric impacts using the coupled TIME-GCM/CCM3, *J. Geophys. Res.*, *107*(D23), 4695, doi:10.1029/2001JD001533.

Liu, H.-L., E. R. Talaat, R. G. Roble, R. S. Lieberman, D. M. Riggin, and J.-H. Yee (2004), The 6.5-day wave and its seasonal variability in the middle and upper atmosphere, *J. Geophys. Res.*, *109*, D21112, doi:10.1029/2004JD004795.

Liu, G., T. J. Immel, S. L. England, K. K. Kumar, and G. Ramkumar (2010), Temporal modulation of the four-peaked longitudinal structure of the equatorial ionosphere by the 2 day planetary wave, *J. Geophys. Res.*, *115*, A12338, doi:10.1029/2010JA016071.

Meier, R., G. Crowley, D. J. Strickland, A. B. Christensen, L. J. Paxton, D. Morrison, and C. L. Hackert (2005), First look at the 20 November 2003 superstorm with TIMED/GUVI: Comparisons with a thermospheric global circulation model, *J. Geophys. Res.*, *110*, A09S41, doi:10.1029/2004JA010990.

Mayr, H. G., and H. Volland (1972), Theoretical model for the latitude dependence of the thermospheric annual and semiannual variations, *J. Geophys. Res.*, *77*(34), 6774–6790, doi:10.1029/JA077i034p06774.

Moudden, Y., and J. M. Forbes (2014), Quasi-two-day wave structure, interannual variability and tidal interactions during the 2002–2011 decade, *J. Geophys. Res. Atmos.*, *119*, 2241–2260, doi:10.1002/2013JD020563.

Onohara, A. N., I. S. Batista, and H. Takahashi (2013), The ultra-fast Kelvin waves in the equatorial ionosphere: Observations and modeling, *Ann. Geophys.*, *31*, 209–215, doi:10.5194/angeo-31-209-2013.

Palo, S. E., R. G. Roble, and M. E. Hagan (1999), Middle atmosphere effects of the quasi-two day wave from a general circulation model, *Earth Planets Space*, *51*, 629–647.

Palo, S. E., J. M. Forbes, X. Zhang, J. M. Russell III, and M. G. Mlynczak (2007), An eastward propagating two-day wave: Evidence for nonlinear planetary wave and tidal coupling in the mesosphere and lower thermosphere, *Geophys. Res. Lett.*, *34*, L07807, doi:10.1029/2006GL027728.

Pancheva, D. V. (2000), Evidence for non-linear coupling of planetary waves and tides in the lower thermosphere over Bulgaria, *J. Atmos. Sol. Terr. Phys.*, *62*, 115–132.

Pancheva, D. V., et al. (2006), Two-day wave coupling of the low-latitude atmosphere-ionosphere system, *J. Geophys. Res.*, *111*, A07313, doi:10.1029/2005JA011562.

Pedatella, N. M., and J. M. Forbes (2012a), The quasi 2 day wave and spatial-temporal variability of the OH emission and ionosphere, *J. Geophys. Res.*, *117*, A01320, doi:10.1029/2011JA017186.

Pedatella, N. M., M. E. Hagan, and A. Maute (2012b), The comparative importance of DE3, SE2, and SPW4 on the generation of wavenumber-4 longitude structures in the low-latitude ionosphere during September equinox, *Geophys. Res. Lett.*, *39*, L19108, doi:10.1029/2012GL053643.

Picone, J. M., R. R. Meier, and J. T. Emmert (2013), Theoretical tools for studies of low-frequency thermospheric variability, *J. Geophys. Res. Space Physics*, *118*, 5853–5873, doi:10.1002/jgra.50472.

Pfister, L. (1985), Baroclinic instability of easterly jets with applications to the summer mesosphere, *J. Atmos. Sci.*, *42*, 313–330.

Plumb, R. A. (1983), Baroclinic instability of the summer mesosphere: A mechanism for the quasi-two-day wave?, *J. Atmos. Sci.*, *40*, 262–270, doi:10.1175/1520-0469(1983)040<0262:BIOTSM>2.0.CO;2.

Plumb, R. A., R. A. Vincent, and R. L. Craig (1987), The quasi-2-day wave event of January 1984 and its impact on the mean mesospheric circulation, *J. Atmos. Sci.*, *44*, 3030–3036.

Qian, L., S. C. Solomon, and T. J. Kane (2009), Seasonal variation of thermospheric density and composition, *J. Geophys. Res.*, *114*, A01312, doi:10.1029/2008JA013643.

Remsberg, E. G., E. R. Lingenfelser, V. L. Harvey, W. Grose, J. Russell III, M. Mlynczak, and L. Gordley (2003), On verification of the quality of SABER temperature, geopotential height, and wind fields by comparison with Met Office assimilated analyses, *Geophys. Res. Lett.*, *108*(D20), 4628, doi:10.1029/2003JD003720.

Salby, M. L., and P. F. Callaghan (2001), Seasonal amplification of the 2-day wave: Relationship between Normal Mode and Instability, *J. Atmos. Sci.*, *58*, 1858–1869.

Strickland, D. J., J. S. Evans, and L. J. Paxton (1995), Satellite remote sensing of thermospheric O/N2 and Solar EUV: 1. Theory, *J. Geophys. Res.*, *100*(A7), 12,217–12,226, doi:10.1029/95JA00574.

Strickland, D. J., R. R. Meier, A. B. Christensen, D. Morrison, L. J. Paxton, S. Avery, J. Craven, G. Crowley, C.-I. Meng, and R. L. Walterscheid (2004), Quiet-time seasonal behavior of the thermosphere seen in the far ultraviolet dayglow, *J. Geophys. Res.*, *109*, A01302, doi:10.1029/2003JA010220.

Teitelbaum, H., and F. Vial (1991), On tidal variability induced by nonlinear interaction with planetary waves, *J. Geophys. Res.*, *96*, 14,169–14,178.

Tunbridge, V. M., D. J. Sandford, and N. J. Mitchell (2011), Zonal wavenumbers of the summertime 2-day planetary wave observed in the mesosphere by EOS Aura MLS, *J. Geophys. Res.*, *116*, D11103, doi:10.1029/2010JD014567.

Wu, D. L., P. B. Hays, and W. R. Skinner (1995), A least squares method for spectral analysis of space-time series, *J. Atmos. Sci.*, *52*, 3501–3511.

Wu, Q., T. L. Killeen, D. A. Ortland, S. C. Solomon, R. D. Gablehouse, R. M. Johnson, W. R. Skinner, R. J. Niciejewski, and S. J. Franke (2006), TIMED Doppler interferometer (TIDI) observations of migrating diurnal and semidiurnal tides, *J. Atmos. Sol. Terr. Phys.*, *68*, 408–417, doi:10.1016/j.jastp.2005.02.031.

Wu, Q., D. A. Ortland, S. C. Solomon, W. R. Skinner, and R. J. Niciejewski (2011), Global distribution, seasonal, and inter-annual variations of mesospheric semidiurnal tide observed by TIMED TIDI, *J. Atmos. Sol. Terr. Phys.*, *73*, 2482–2502, doi:10.1016/j.jastp.2011.08.007.

Xu, J., W. Wang, and H. Gao (2013), The longitudinal variation of the daily mean thermospheric mass density, *J. Geophys. Res. Space Physics*, *118*, 515–523, doi:10.1029/2012JA017918.

Yamazaki, Y., and A. D. Richmond (2013), A theory of ionospheric response to upward-propagating tides: Electrodynamic effects and tidal mixing effects, *J. Geophys. Res. Space Physics*, *118*, 5891–5905, doi:10.1002/jgra.50487.

Yue, J., H.-L. Liu, and L. C. Chang (2012a), Numerical investigation of the quasi 2 day wave in the mesosphere and lower thermosphere, *J. Geophys. Res.*, *117*, D05111, doi:10.1029/2011JD016574.

Yue, J., W. Wang, H.-L. Liu, and A. Richmond (2012b), Quasi-two-day wave coupling of the mesosphere and lower thermosphere-ionosphere in the TIME-GCM: Two-day oscillations in the ionosphere, *J. Geophys. Res.*, *117*, A07305, doi:10.1029/2012JA017815.

Yue, J., W. Wang, A. D. Richmond, H.-L. Liu, and L. C. Chang (2013a), Wavenumber broadening of the quasi 2 day planetary wave in the ionosphere, *J. Geophys. Res. Space Physics*, *118*, 3515–3526, doi:10.1002/jgra.50307.

Yue, J., J. Xu, L. C. Chang, Q. Wu, H.-L. Liu, X. Lu, and J. Russell III (2013b), Global structure and seasonal variability of the migrating terdiurnal tide in the mesosphere and lower thermosphere, *J. Atmos. Sol. Terr. Phys.*, *105-106*, 191–198, doi:10.1016/j.jastp.2013.10.010.

Yue, J., and W. Wang (2014), Changes of thermospheric composition and ionospheric density caused by quasi two-day wave dissipation, *J. Geophys. Res. Space Physics*, *119*, 2069–2078, doi:10.1002/2013JA019725.

Zhang, X., J. M. Forbes, M. E. Hagan, J. M. Russell III, S. E. Palo, C. J. Mertens, and M. G. Mlynczak (2006), Monthly tidal temperatures 20–120 km from TIMED/SABER, *J. Geophys. Res.*, *111*, A10S08, doi:10.1029/2005JA011504.

Zhang, Y., and L. J. Paxton (2011), Long-term variation in the thermosphere: TIMED/GUVI observations, *J. Geophys. Res.*, *116*, A00H02, doi:10.1029/2010JA016337.